UDK 621.315.592

Terahertz radiation detector based on thermoelectric material $Bi_{88}Sb_{12}$*

© E.S. Makarova[1], A.V. Asach[1], I.L. Tkhorzhevskiy[1], A.D. Sedinin[1], D.V. Zykov[1], A.D. Zaitsev[1], P.S. Demchenko[1], M.G. Novoselov[1], V.A. Komarov[2], A.S. Tukmakova[1], A.V. Novotelnova[1], N.S. Kablukova[1,3], M.K. Khodzitsky[1]

[1] ITMO University,
197101 St. Petersburg, Russia
[2] Herzen State Pedagogical University of Russia,
191186 St. Petersburg, Russia
[3] St. Petersburg State University of Industrial Technologies and Design,
191186 St. Petersburg, Russia

E-mail: makarova_helena_2011@mail.ru

Received September 24, 2021
Revised November 20, 2021
Accepted November 20, 2021

Terahertz radiation is very promising for visualization, detection and data transfer. Searching for sensitive, fast and compact THz detector that operates at room temperature is a common subject for these applications. Hence, there is still an issue of searching for new materials for THz radiation detection. Solid solutions based on thermoelectric bismuth and antimony appear to have significant potential for these applications. In this paper photoresponse of thermoelectric material $Bi_{88}Sb_{12}$ has been studied for the first time. Films with thicknesses of 70 and 150 nm were studied under influence of radiation at frequency of 0.14 THz.

Keywords: terahertz radiation, photoresponse, bismuth, antimony, thermoelectric materials, thin films.

DOI: 10.21883/SC.2022.04.53229.7a

1. Introduction

Terahertz (THz) radiation is very promising for solving various practically important problems and can be used in spectroscopy [1], visualization [2], detection and data transfer systems [3]. For THz technologies the problem associated with the lack of available and efficient terahertz devices is relevant [4]. So, despite the fact that over the past two decades a significant amount of researches has been devoted to the development of a highly sensitive, fast, compact detector THz radiation operating at room temperature, many open problems remain in this direction [5]. One of the main tasks is to search for new materials with high sensitivity to THz radiation at room temperature, for their use as a functional medium in detection systems. Most of the currently proposed terahertz sensors either have a high response speed, but have a low sensitivity, or have a high sensitivity with a low speed [6].

Thermoelectric materials based on bismuth and antimony solid solutions have a significant potential for solving this problem [7]. Due to their small band gap, they belong to the semimetals class with good thermoelectric characteristics. Absorption of THz radiation by semimetals results in the appearance of additional pairs of charge carriers due to the absorption of energy sufficient to transfer an electron to the conduction band, that is similar to the appearance of hot electrons (holes) in the thermoelectric effect. The signal generated by the photothermoelectric effect can be amplified. To do this, it is necessary to use a material with the maximum thermoelectric figure of merit for a given ambient temperature [8].

In this study, we study the response in the thermoelectric films $Bi_{88}Sb_{12}$ with a thickness of 70 and 150 nm upon absorption of THz radiation of different polarizations depending on the distance between generator and detector. The detector operation under the application of an external electric field is also analyzed.

2. Materials and methods

2.1. Samples preparation

For the study the samples of bismuth–antimony solid solution films were obtained on the mica with the thickness of 21 μm. Films were produced by thermal evaporation in vacuum. Discrete evaporation was used to obtain films of the uniform composition throughout the entire volume. The films were formed in vacuum at a pressure of $2 \cdot 10^{-3}$ Pa. All films were obtained in the similar technological modes: during the deposition of the substance, the substrate temperature was maintained at 393 K, then they were annealed directly in the evaporation chamber under vacuum at a temperature of 493 K for 30 minutes. As a result, bismuth–antimony solid solution films were obtained with the dimensions of 0.8×1 mm, thicknesses of 150 and 70 nm, and an antimony concentration of 12%. The film thickness was measured by means of

* Report at XXVII Interstate conference „Thermoelectric materials and their applications“ (ISCTA 2021), Saint Petersburg, September 13–16, 2021.

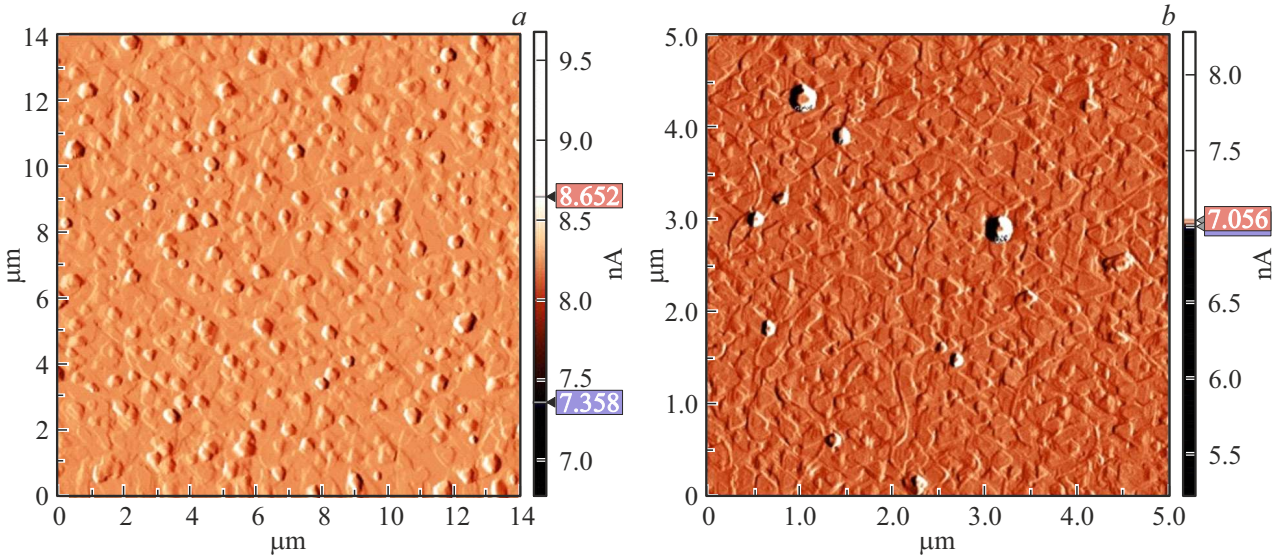

Figure 1. AFM-image of $Bi_{88}Sb_{12}$ film surface on mica; film thickness: *a* — 150 nm, *b* — 70 nm.

optical interferometry using a Linnik interferometer MII-4 (measurement error does not exceed 5 nm). The film structure was analyzed using the atomic-force microscopy (AFM) method. The study was performed on a scanning probe microscope Solver P47-PRO in the semi-contact mode. Fig. 1 demonstrates the relief of $Bi_{88}Sb_{12}$ films with the thickness of 150 and 70 nm. The films have two types of inhomogeneities: convex three-dimensional formations in the form of a pimple and triangular growth patterns. The triangular texture reflects the rhombohedral crystalline structure Bi [9]. This form of growth patterns indicates, that the crystallographic orientation of this film corresponds to the direction of the C_3 axis parallel to the film normal [10,11], and C_1 and C_2 axes lie in the substrate plane and they are parallel and oppositely directed in neighboring crystallites [12]. According to mutual position of growth patterns on the film surface the size of film crystallites is determined [11,13]: for 150 nm film the size of crystallites can reach 3 μm (see Fig. 1, *a*), for 70 nm film the size of crystallites does not exceed 1.5–2 μm (see. Fig. 1, *b*).

2.2. Expected effects and phenomena

When a substance absorbs electromagnetic radiation, an internal photoelectric effect will appear, in case the radiation quantum energy is sufficient to transfer electrons from the valence band to the conduction band. This condition is satisfied under condition of interaction of the $Bi_{88}Sb_{12}$ solid solution with THz radiation in a wide frequency range from 0.1 to 10 THz. The study [14] showed, that the charge carrier plasma frequency, which determines the upper frequency limit of the possibility of detecting radiation, in bulk bismuth lies within the range from 93 to 99 THz (depending on the radiation polarization) at the temperature of 300 K. In case of cooling to the temperature of 80 K the plasma frequency decreases to the values of 59–62 THz, that is in good agreement with the results of the study [15], in which the features of the reflection spectra of doped bismuth–antimony crystals were studied in the long-wave infrared spectrum. However, as shown in the study [16], with a decrease in the bismuth film thickness up to the values of 40 to 150 nm at a temperature of 300 K a decrease in the plasma frequency (compared to bulk samples) up to 55 THz at a thickness of 40 nm and up to 67 THz at a thickness of 150 nm is also observed. Consequently, under the effect of monochromatic radiation of 0.14 THz in $Bi_{88}Sb_{12}$ at 300 K the radiation absorption will be observed, and to describe the processes the theory of internal photoeffect for semiconductors may be used. The film conductivity may be described by the formula

$$\sigma = \sigma_0 + \Delta\sigma = q\mu_e n_{0e} + q\mu_p n_{0p} + (q\mu_e n_{de} + q\mu_p n_{dp}), \quad (1)$$

where σ_0 and $\Delta\sigma$ — dark conductivity and photoconductivity, n_{0e} and n_{0p} — concentrations of electrons and holes respectively, n_{de} and n_{dp} – concentrations of the generated by radiation electron-hole pairs, μ_e and μ_p — charge mobility, q — electron charge modulus.

2.3. Experimental technique

In this study the experiments on study of the response in $Bi_{88}Sb_{12}$ solid solution films at the absorption of terahertz radiation were carried out. The influence of the applied voltage magnitude, the polarization angle of the incident radiation, and the distance from the radiation source to the film on the internal photoeffect were studied. The idea of the experiment was the successive photoexcitation of nonequilibrium charge carriers. As a source of terahertz

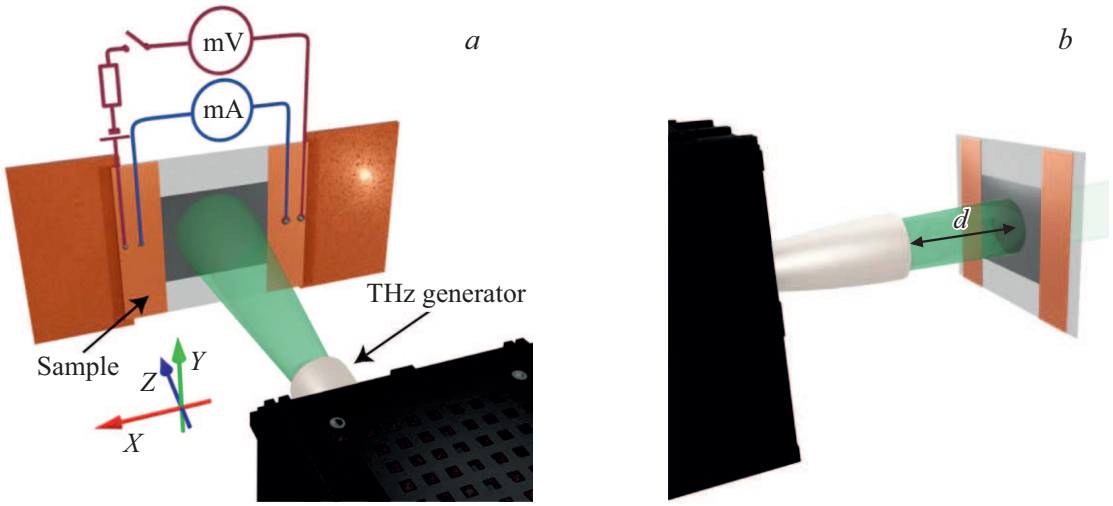

Figure 2. Installation scheme: *a* — polarization orientation and four-probe method, *b* — change in the distance between the source and film.

radiation, a commercial source of continuous radiation with a frequency of 0.14 THz and power 30 mW of Terasense brand was used. The photo-emf induced by terahertz radiation was recorded by means of the four-probe method (Fig. 2). From a 1.5 V constant voltage source a current was applied through the sample and a resistance box up to 5 kOhm, which did not lead to the heating of the sample. The measurements were carried out at two orientations of the polarization of the electric field vector of THz radiation: parallel and perpendicular to the current flow direction. In the first series of experiments thin $Bi_{88}Sb_{12}$ films were studied at terahertz radiation with a flowing direct current along the films. The photoresponse was recorded with a Keithley DMM7510 millivoltmeter.

In the second series of experiments, due to the (d) distance between horn antenna of THz radiation source and the film surface, the standing THz wave was registered. Since the standing wave arises due to multiple reflections between the horn and the sample, it is assumed that the response measured by a millivoltmeter in proportion to the radiation power, will vary with the distance between the sample and the source. In this case as long as d increases from 0 to 1500 μm, several minima and maxima of signal power values appear with a period of $\lambda/2$ (where the wavelength is $\lambda \approx 2141\,\mu$m).

3. Results

Figures 3 and 4 show the characteristic dependence of the voltage drop across the sample in the absence and presence of radiation. For the films a constant current was maintained: for 150 and 70 nm films the current was 0.107 mA and 0.010 mA.

In Figures $3,a$ and $4,a$ for a 70 nm film two voltage dependences of time, which show the effect of radiation polarization, are shown. Figures $3,b$ and $4,b$ show the dependence of the voltage drop in the films at the perpendicular direction of radiation polarization to the current passing through the film. Based on the analysis of the data presented in Fig. 3 and 4, one can calculate the specific photoconductivity using the voltage drop difference in all the cases presented using the formula

$$\Delta\sigma = \frac{I}{\Delta U} \cdot \frac{L}{S}, \tag{2}$$

where $\Delta\sigma$ — photoconductivity, I — current, ΔU — photo-emf, L — film length, S — the cross-sectional area of the film.

For a 70 nm film (Fig. $3,a$) one can notice a significant difference in the voltage drop for different polarization directions. If the radiation polarization is perpendicular to the current direction ($\mathbf{E} \perp \mathbf{I}$), then $\Delta U = -0.089$ mV, and the specific photoconductivity is $\Delta\sigma_1 = 1.28 \cdot 10^6\,(\text{Ohm} \cdot \text{m})^{-1}$. If the radiation polarization is parallel to the current direction ($\mathbf{E} \parallel \mathbf{I}$), then $\Delta U = -0.101$ mV, and the specific photoconductivity is $\Delta\sigma_2 = 1.13 \cdot 10^6\,(\text{Ohm} \cdot \text{m})^{-1}$. Different results of $\Delta\sigma_1$ and $\Delta\sigma_2$ indicate the influence of the radiation polarization direction on the mobility of charge carriers. Such a behavior of the radiation polarization dependence was observed in all the experiments performed.

For a 150 nm film (Fig. $3,b$) and a polarization perpendicular to the current direction ($\mathbf{E} \perp \mathbf{I}$), the photo-emf value is $\Delta U = -0.067$ mV, and the specific photoconductivity is $\Delta\sigma_3 = 0.85 \cdot 10^6\,(\text{Ohm} \cdot \text{m})^{-1}$. When comparing the magnitude of the response from the films of different thicknesses (see Fig. $3,b$), it is noticeable that the signal from a thicker film is larger, but the photo-emf value is 0.022 mV less than from 70 nm film. This effect can be associated with a small change in the electronic spectrum due to the film thickness.

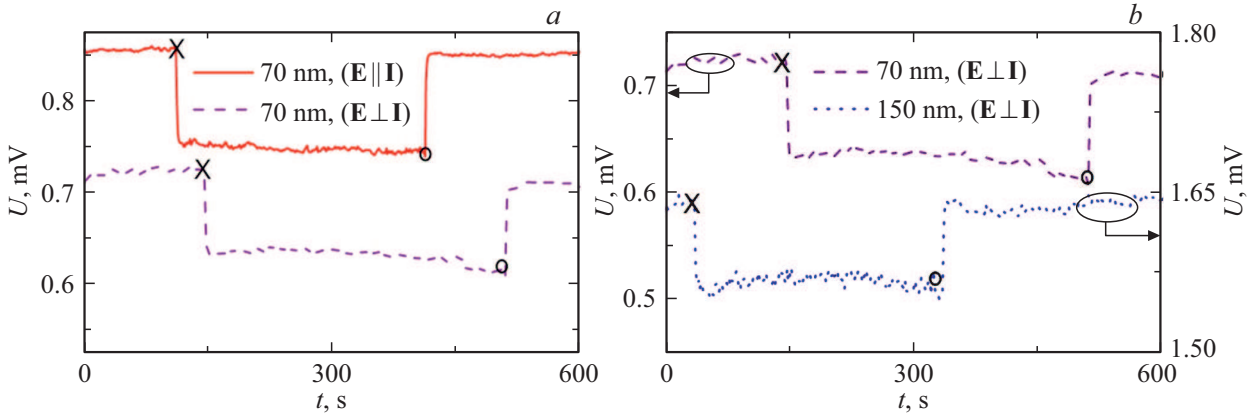

Figure 3. Time dependences of the voltage drop on 70 and 150 nm films: *a* — for a 70 nm film at different polarization directions; *b* — for 70 and 150 nm films at perpendicular radiation polarization direction. The graph shows the moments of switching-on (×) and switching off (○) the dropping voltage.

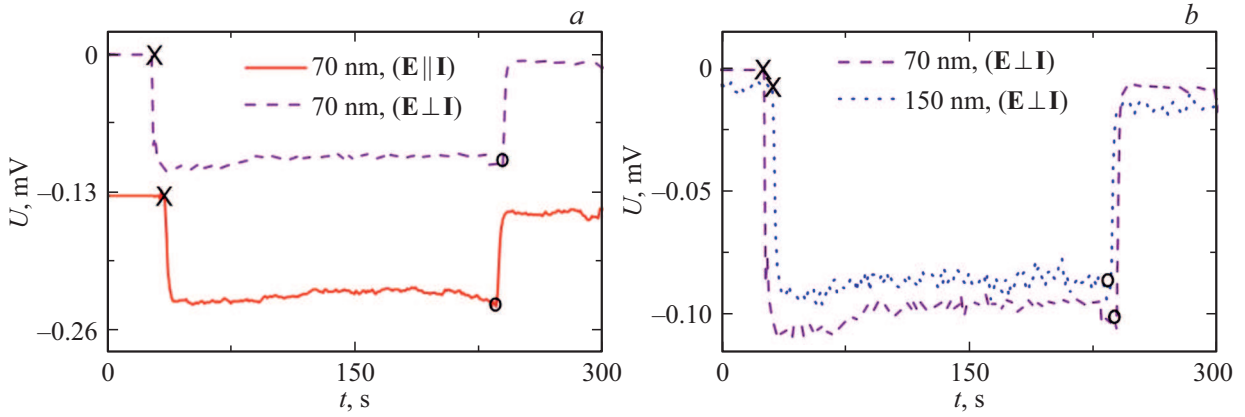

Figure 4. Time dependence of the photo-emf in 70 and 150 nm films. No current through the sample: *a* — for a 70 nm film at different polarization directions; *b* — for 70 and 150 nm films at perpendicular radiation polarization direction. The graph shows the moments of switching-on (×) and switching off (○) the dropping voltage.

Figure 4, *a* for a 70 nm film shows the dependence of the photo-emf of radiation polarization direction. When the radiation polarization is perpendicular to the current axis ($\mathbf{E} \perp \mathbf{I}$), then the photo-emf is $\Delta U = -0.10$ mV, and the radiation polarization is parallel to the current axis ($\mathbf{E} \parallel \mathbf{I}$) — $\Delta U = -0.22$ mV. For a 150 nm film (Fig. 4, *b*) with perpendicular polarization, the photo-emf value is -0.09 mV. Fig. 4 demonstrates well the drift of charge carriers behind the intensity of the radiation electric field ($\mathbf{E} \parallel \mathbf{I}$), since there is no other effect on charge carriers, except for THz radiation.

4. Investigation of the dependence of the response to THz radiation on the distance between generator and sample

When radiation is normally incident on the $Bi_{88}Sb_{12}$ film, the effect of standing waves arises due to the superposition of the incident and reflected waves in the space in front of the detector. This results in the change in the radiation power in the space between generator and detector. The sample was fixed at given points in space from the radiation source (see Fig. 2, *b*), then the experiment described above was carried out in this position. In Fig. 5 one can clearly see the decrease in the photo-emf at a certain point in space, i.e. there is a decrease in energy, and consequently, a node of a standing wave appears. Since $\sim 25\%$ of radiation is reflected from the detector surface, it is necessary to deflect the detector by a small angle to avoid wave interference, which can lead to both frequency-dependent and space-dependent modulation of the detected radiation power.

The dependence of the induced photocurrent on the orientation of linearly polarized radiation for two-dimensional materials, to which, with some approximation, the samples of interest in this study can be attributed (due to the small ratio of the film thickness to the radiation wavelength), has a cosine character [17], that cab be also seen in Fig. 5. Based on the assumption of a linear dependence of the

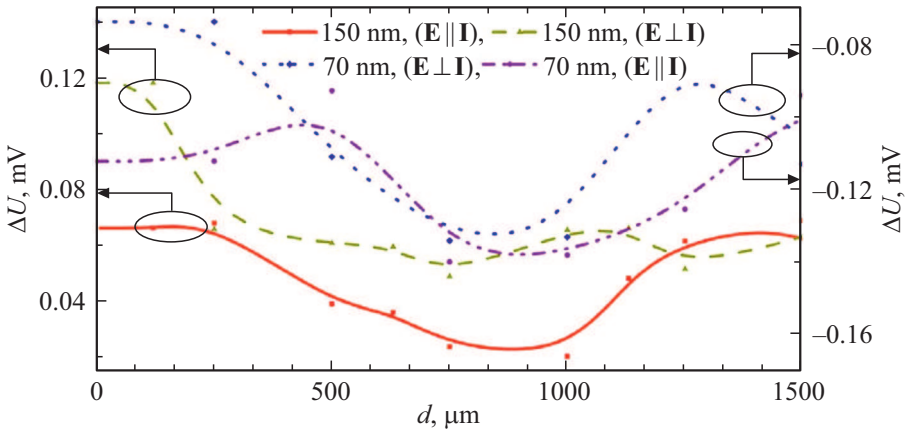

Figure 5. Photo-emf dependence in 70 and 150 nm films of the distance and radiation polarization.

photocurrent (photo-emf) on the intensity of the incident light radiation, it can be argued that the photocurrent depends cosinusoidally on the angle of the polarization plane:

$$I_{\text{ph}} = a \cdot \cos(2\theta + \theta_0) + I_0, \qquad (3)$$

where θ_0 — initial phase.

Thus, by choosing $\theta_0 = 0°$, one can observe the maximum value of the photocurrent at $\theta_0 = 0°$ and the minimum value at $\theta = 90°$.

5. Conclusion

The detector presented in this study is a promising compact and inexpensive alternative to the existing detectors, which are used to detect THz radiation at room temperature. This technology can be integrated into multipixel detector matrices at large scale, that allows to create a compact and cost-effective THz imaging systems. A big advantage of these THz detectors is the relatively easy scalability of the detection frequency, due to the fact that both the thermoresistive effect and the thermoelectric effect are broadband.

Funding

The researches are supported by RSF grant, project No. 19-72-10141.

Conflict of interest

The authors declare that they have no conflict of interest.

References

[1] P. Bawuah, J.A. Zeitler. Trends Anal. Chem., **139**, 116272 (2021).
[2] A. Bandyopadhyay, A. Sengupta. IETE Tech. Rev., **1**–**19** (2021).
[3] H. Rahaman, A. Bandyopadhyay, S. Pal, K.P. Ray. IETE Tech. Rev., **1**–**14** (2020).
[4] S.S. Dhillon, M.S. Vitiello, E.H. Linfield, A.G. Davies, M.C. Hoffmann et al. J. Phys. D: Appl. Phys., **50** (4), 043001 (2017).
[5] F. Sizov. Semicond. Sci. Technol., **33**, 123001 (2018).
[6] R.A. Lewis. J. Phys. D: Appl. Phys., **52**, 433001 (2019).
[7] A.D. Zaitsev, P.S. Demchenko, D.V. Zykov, E.A. Korotina, E.S. Makarova, I.L. Tkhorzhevskiy, A.S. Tukmakova, N.S. Kablukova, A.V. Asach, A.V. Novotelnova, M.K. Khodzitsky. Appl. Sci., **10** (8), 2724 (2020).
[8] M.K. Khodzitsky, P.S. Demchenko, D.V. Zykov, A.D. Zaitsev, E.S. Makarova, A.S. Tukmakova, I.L. Tkhorzhevskiy, A.V. Asach, A.V. Novotelnova, N.S. Kablukova. Photonics, **8** (3), 76 (2021).
[9] T.-R. Chang, Q. Lu, X. Wang, H. Lin, T. Miller, T.-C. Chiang, G. Bian. Crystals, **9** (10), 510 (2019).
[10] V.M. Grabov et al. J. Thermoelectr., **1**, 41 (2009).
[11] V.M. Grabov, E.V. Demidov, V.A. Komarov, M.M. Klimantov. FTT, **51** (4), 800 (2009) (in Russian).
[12] V.M. Grabov, E.V. Demidov, V.A. Komarov. FTT, **52** (6), 1219 (2010) (in Russian).
[13] V.M. Grabov, E.V. Demidov, V.A. Komarov. FTT, **50** (7), 1312 (2008) (in Russian).
[14] E. Gerlach, M. Rautenberg. Phys. Status Solidi B, **75** (2), 553 (1976).
[15] V.M. Grabov, N.P. Stepanov. FTP, **35** (2), 155 (2001) (in Russian).
[16] A. Zaitsev, P.S. Demchenko, M.K. Khodzitsky, E.S. Makarova, A.S. Tukmakova, A.V. Asach, A.V. Novotelnova, N.S. Kablukova. Phys. Status Solidi Rapid Res. Lett., **14** (7), 2000093 (2020).
[17] F. Chu, M. Chen, Y. Wang, Y. Xie, B. Liu, Y. Yang, X. An, Y. Zhang. J. Mater. Chem. C, **6** (10), 2509 (2018).

Editor A.N. Smirnov